Lasers Med Sci (2011) 26:133–138
DOI 10.1007/s10103-010-0831-8

BRIEF REPORT

Scanning electron microscopy (SEM) and X-ray dispersive spectrometry evaluation of direct laser metal sintering surface and human bone interface: a case series

Carlo Mangano · Adriano Piattelli · Mario Raspanti · Francesco Mangano · Alessandra Cassoni · Giovanna Iezzi · Jamil Awad Shibli

Received: 15 December 2009 / Accepted: 7 August 2010 / Published online: 28 August 2010

Abstract Recent studies have shown that direct laser metal sintering (DLMS) produces structures with complex geometry and consequently that allow better osteoconductive properties. The aim of this patient report was to evaluate the early bone response to DLMS implant surface retrieved from human jaws. Four experimental DLMS implants were inserted in the posterior mandible of four patients during conventional dental implant surgery. After 8 weeks, the micro-implants and the surrounding tissue were removed and prepared for scanning electron microscopy (SEM) and histomorphometric analysis to evaluate the bone–implant interface. The SEM and EDX evaluations showed a newly formed tissue composed of calcium and phosphorus. The bone-to-implant contact presented a mean of 60.5±11.6%. Within the limits of this patient report, data suggest that the DLMS surfaces presented a close contact with the human bone after a healing period of 8 weeks.

Keywords Dental implants · Human histology · Implant surface topography · Laser manufacturing · Osseointegration · Wound healing

C. Mangano
Department of Biomaterials, University of Insubria-Varese, Varese, Italy

A. Piattelli
Department of Oral Medicine and Pathology, University of Chieti, Chieti, Italy

M. Raspanti
Department of Human Morphology, University of Insubria-Varese, Varese, Italy

F. Mangano
Como, Italy

A. Cassoni
Department of Restorative Dentistry, Guarulhos University, Guarulhos, SP, Brazil

G. Iezzi
University of Chieti, Chieti, Italy

J. A. Shibli (✉)
Department of Periodontology, Dental Research Division, Guarulhos University, 07011-040 Guarulhos, SP, Brazil
e-mail: jashibli@yahoo.com

Introduction

Dental implant placement is now in widespread use for oral rehabilitation treatment. The main reason for the high success rates is the recent advances in the macro- and micro-geometry of the implants. The micro-geometry plays a pivotal role in bone-to-implant contact and, consequently, in the success of the implant-supported restoration. The reaction of the cells to implant surface at micrometer scale features have been well established [1, 2]. Previous studies [3–6] demonstrated that rough implant surface topography at the micrometer scale presented better osteogenic response compared to as-machined dental implant surface.

However, it has been shown that porous implant surface can be designed to closely mimic the natural structure and mechanical properties of bone tissue compared to their solid-cast counterparts [7, 8]. Consequently, conventional

manufacturing methods are difficult to employ in producing such porous devices with tight constrains of several physical and chemical characteristics [9].

The direct laser metal sintering (DLMS) process is a technology that produces solid metal components with intricate porous geometries [10–13]. Recently, Mangano et al. [12] have shown that DLMS produces structures with complex geometry that consequently allow better osteoconductive properties. Cytocompatibility and fibrin clot extension evaluations were carried out using osteoblasts and human whole blood to compare cell growth and covered area by fibrin clot on several implants surfaces topographies. DLMS surface depicted a similar cell density to that on commercial rough surface but lower than on as-machined and smooth-textured grit-blasted, acid-etched surfaces. In addition, the extension of human blood clot was slightly improved by inorganic acid etching on DLMS surface to increase the microroughness. Moreover, it was shown that implants obtained through laser metal sintering were better adapted to the elastic properties of bone [11]. Therefore, DLMS implants could not only minimize stress-shielding effects but also improve implant long-term success rates. These observations suggested that the direct laser fabrication technique is a promising economical method for producing implants from commercially pure titanium or alloys. However, the quantity of bone–implant contact percentage and the quality of the bone–implant interface around these surfaces is currently under research.

Therefore, the aim of this case series was to evaluate, by scanning electron microscopy (SEM), X-ray dispersive spectrometry and histology, the human bone response to DLMS implant surface topographies after an unloaded healing period of 8 weeks.

Materials and methods

Subjects

Four partially edentulous subjects (three women, one man), with a mean age±SD of 51.3±12.45 years, referred to the Oral Implantology Clinic, Guarulhos University, Brazil, for oral rehabilitation with dental implants were included in this report. Exclusion criteria included pregnancy, nursing, smokers, and any systemic condition that could affect bone healing. The Ethics Committee for Human Clinical Trials at Guarulhos University approved the study protocol.

Implant preparation

Screw-shaped micro-implants (2.5 mm in diameter and 6.0 mm long) were prepared with direct laser metal sintering surface. These implants were made of master alloy powder, Ti-6Al-4V (Leader Implants, Novaxa, Milan, Italy) with a particle size of 25–45 μm as the basic material. Processing was carried out in an argon atmosphere using a powerful Yb (ytterbium) fiber laser system (EOS GmbH, Munich, Germany) with the capacity to build a volume up to 250× 250 × 215 mm using a wavelength of 1,054 nm with a continuous power of 200 W, at a scanning rate of 7 m/s. The size of the laser spot was 0.1 mm. To remove residual particles from the manufacturing process, the samples were sonicated for 5 min in distilled water at 25°C, immersed in NaOH (20 g/l) and hydrogen peroxide (20 g/l) at 80°C for 30 min, and then further sonicated for 5 min in distilled water. Acid etching was carried out by immersion of the samples in a mixture of 50% oxalic acid and 50% maleic acid at 80°C for 45 min, washing for 5 min in distilled water in a sonic bath. Following these procedures, the implants were sterilized in gamma radiation and stored in appropriate packs.

Implant surface characterization

An optical laser profilometer (Mahr GmbH, Gottingen, Germany) was used to measure and characterize the dental implant surface topography. Eight micro-implants were measured three times each on the side, top, and bottom. The measured parameters, such as the arithmetic average of all profile point absolute values (Ra), the root-mean-square of all point values (Rq), and the average absolute height values of the five highest peaks and the depths of the five deepest valleys (Rz) were measured in all specimens.

Micro-implants surgery

Four micro-implants were used in this case series. Each subject received one micro-implant, which was inserted in the mandible, always distal to the last conventional placed implant.

The micro-implants were placed under aseptic conditions as previously described [2, 4]. After crestal incision, mucoperiosteal flaps were raised and conventional implants were placed in the mandible in accordance with the surgical/prosthetic plan prepared for each patient. Next, the micro-implant was placed in the molar region, i.e., posterior to the most distal conventional implant (Fig. 1). The micro-implant recipient site was prepared with a 2-mm-diameter twist drill. All drilling and micro-implant placement procedures were completed under profuse irrigation with sterile saline. The flaps were sutured to cover the micro-implants. Clindamycin was administered three times a day (1,200 mg/day) for 1 week, in order to avoid post-surgical infection. The sutures were removed after 10 days. To enable subjects to control

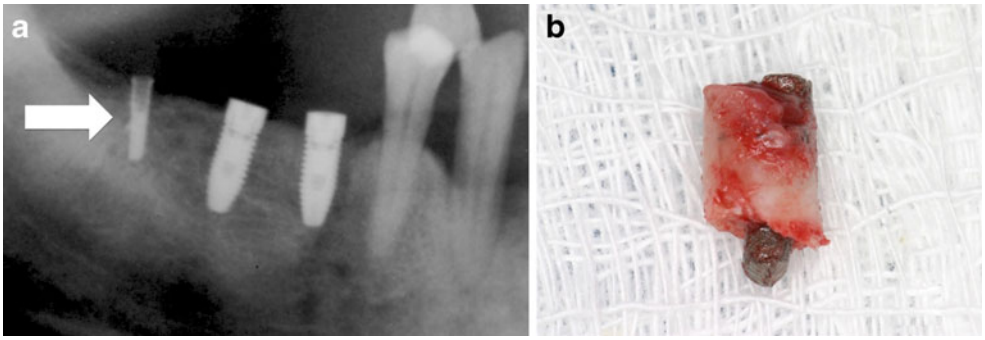

Fig. 1 **a** Radiographic view of the micro-implant (*arrow*) inserted at distal position of the conventional implants. **b** Retrieved implant after 8 weeks of healing

postoperative dental biofilm, 0.12% chlorhexidine rinses were prescribed twice a day for 14 days.

After a healing period of 8 weeks, during the two-stage surgery of the conventional implants, the micro-implants and the surrounding tissues were retrieved with a 4-mm-wide trephine bur, and the specimens were fixed by immediate immersion in neutral formalin at 4%.

Preparation of specimens

Scanning electron microscopy (SEM) and X-ray dispersive spectrometry

Two specimens were washed with Na-cacodylate buffer (pH 7.4), dehydrated in ascending ethanol and hexamethyl-disilazane, sputter-coated with pure gold in an Emitech K550 apparatus and mounted on appropriate stubs with carbon-based conductive adhesive. All specimens were observed under an FEI XL-30 FEG scanning electron microscopy (SEM) operated at 7–15 kV. Pictures were directly acquired in digital format as 1424 x 968-pixel grayscale TIFF images.

X-ray spectrometry was carried out on the same SEM fitted with an EDAX Sirion 200/400 apparatus and operated at 15 kV. Digital maps of the distribution of distinct elements were obtained in digital format as 512 x 512 BMP pictures. Selected maps were combined with the corresponding SEM micrographs in Adobe Photoshop (Adobe Systems, San Jose, CA, USA).

Histometric analysis

The other two remaining biopsies were processed (Precise 1 Automated System®, Assing, Rome, Italy) to obtain thin ground sections as previously described [14]. The specimens were dehydrated in an ascending series of alcohol rinses and embedded in glycol methacrylate resin (Technovit® 7200 VLC, Kulzer, Wehrheim, Germany). After polymerization, the specimens were sectioned lengthwise along the larger axis of the implant, using a high-precision diamond disk, to about 150 μm, and ground down to about 30 μm. Two slides were obtained from each implant. The slides were stained with basic fuchsin and toluidine blue. Bone-to-implant contact (BIC%) was defined as the amount of mineralized bone in direct contact with the implant surface. The measurements were made throughout the entire extent of the micro-implant. This evaluation was performed using a light microscope (Laborlux S®, Leitz, Wetzlar, Germany) connected to a high-resolution video camera (3CCD®, JVC KY-F55B, Milan, Italy) and interfaced to a monitor and personal computer. This optical system was associated with a digitizing pad (Matrix Vision GmbH, Milan, Italy) and a histometry software package with image-capture functionalities (Image-Pro Plus® 4.5, Media Cybernetics Inc., Immagini & Computer Snc, Milan, Italy). The mean and standard deviation of BIC% was calculated for each implant.

Results

Surface roughness parameters

The surface topography of the DLMS had no clear orientation. The direct laser preparation provided an implant surface with roughness surface with the mean± SD of average of the absolute values of all profile points (Ra), the root-mean-square of the values of all points (Rq), and the average value of the absolute heights of the five highest peaks and the depths of the five deepest valleys (Rz) of 66.8±6.6, 77.6±11.1 and 358.3±101.9 μm, respectively.

SEM and EDX results

The SEM analysis showed a diffuse and close contact between the implant surface and the newly formed bone. The mineralized bone tissue ingrowths into the porous and irregularities of the implant surface except on the external implant areas, probably due the implant retrieval procedure. The osteoblasts present a spread configuration with several citoplasmatic extensions (Fig. 2).

The spectroscopy analysis allowed an analysis of the elements presented in the mineralized bone tissue formed

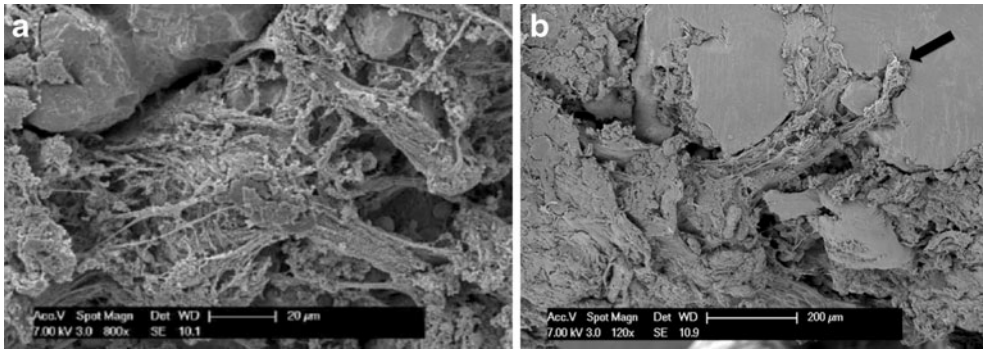

Fig. 2 **a** Scanning electron micrograph showing bone matrix adherent to the orifices of a DLMS surface after 8 weeks of healing. **b** Microphotograph showing bone–implant interface. Bone was broken away to expose the implant surface. Note that there are growing dense mineralized bone matrix inside the complex geometry of the surface (*arrow*)

on the implant surface. The distribution of calcium (Ca), phosphorus (P), and titanium (Ti) is represented by green, red, and blue, respectively. The newly formed bone presented a sparse distribution of Ca and P. When the images were combined, a mineralized tissue structure in close contact with the implant surface was observed (Fig. 3).

Histological and histometric results

The remaining two micro-implants were histologically evaluated. They presented a varied degree of bone attachment, mainly in the coronal aspect. In addition, the specimens showed the presence of remodeling activity in the bone next to the micro-implants, depicting a woven bone with several osteocyte lacunae (Fig. 4). The woven newly formed bone was separated from the preexisting bone by cement lines. Osteoblasts were connected to the newly formed bone, showing ongoing bone formation. The newly formed bone contact was primarily composed of woven bone connecting the peri-implant bony trabeculae to the micro-implant surface. The implant surface showed superficial debris or particle inclusions in the surrounding tissue close to the bone area. BIC% values of the two retrieved implants utilized for histological analysis depicted a mean± SD of 60.5±11.6%.

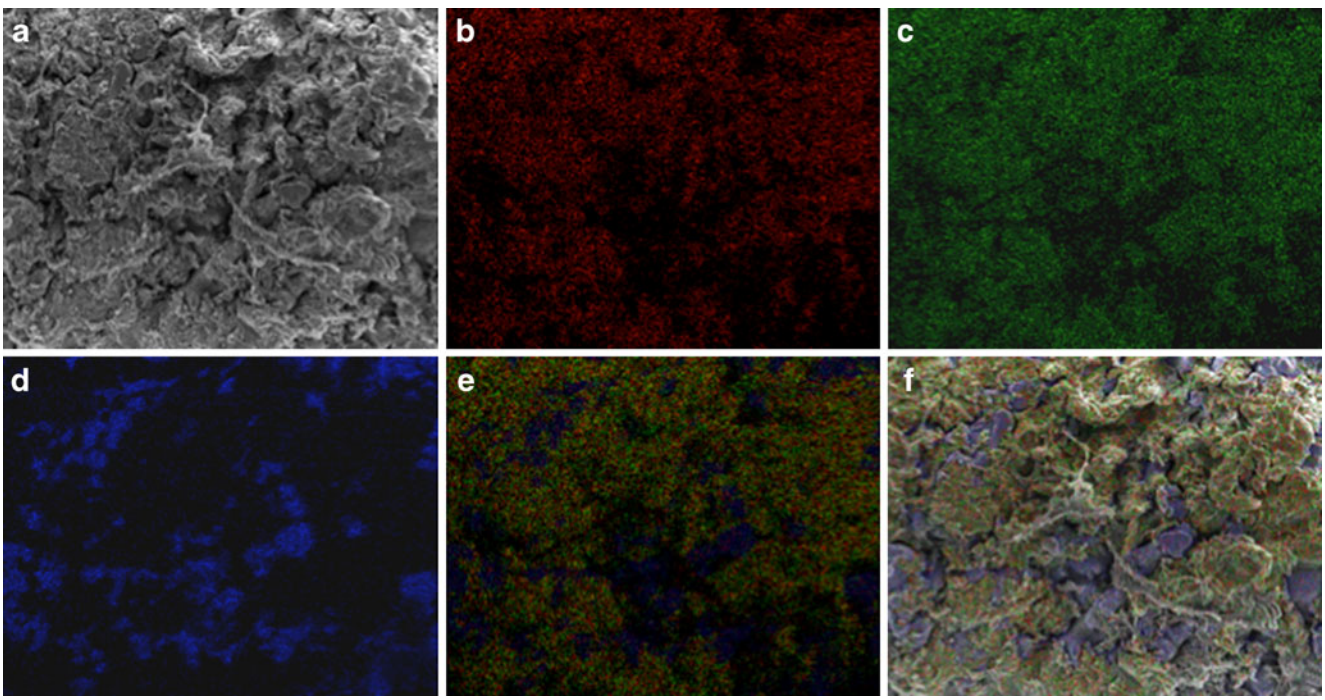

Fig. 3 **a** Microphotography of an area with newly formed bone on DLMS surface (250x). **b** Digital image obtained of **a**. The EDX analysis depicted in *red*, the presence of phosphorus, (**c**) in green calcium and (**d**) titanium in blue (250x). **e** The three images (B+C+D) are superimposed showing a map of the three elements. **f** Combining images E and A, a new map depicting a complete view of the implant surface and the newly formed bone (250x) is shown

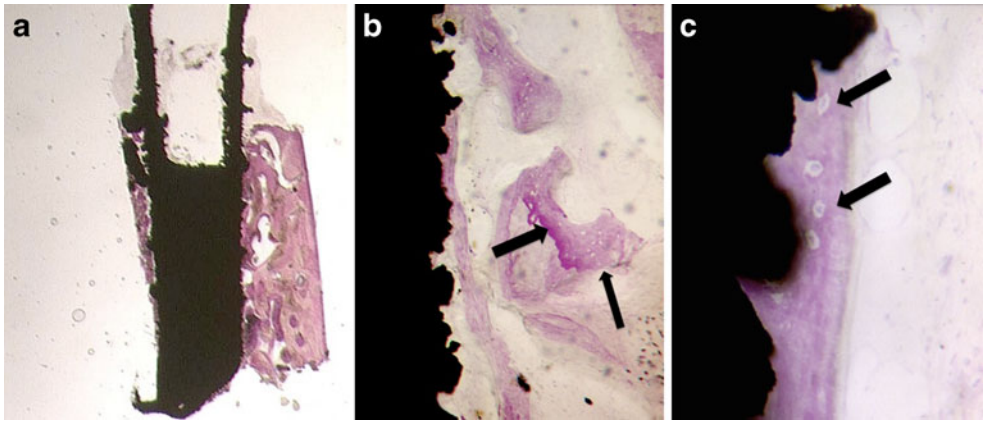

Fig. 4 **a** Histological ground section of the direct laser fabrication micro-implant surface after 8 weeks of healing depicting the newly formed bone showing early maturing stages. There are connecting bridges between the new bone trabeculae and the implant surface (basic fuchsin and toluidine blue staining, original 12x magnification). **b** There are reversal lines (*arrows*) between newly formed bone and the pristine bone (basic fuchsin and toluidine blue staining, original 100x magnification). **c** The newer bone tissue showing their osteocytes (*arrows*) is in close contact with the implant surface (basic fuchsin and toluidine blue staining, original 200x magnification)

Discussion

The present case series presented histologic and SEM evaluation of the bone formation around DLMS implants retrieved from human jaws after 8 weeks of healing. The bone-to-implant contact presented on the DLMS implants retrieved from the mandible was similar to previous reports that evaluated other implant surface topographies [3, 4]. Osteogenic cell migration and new bone apposition allows direct bone formation on the implant surface topography. The first step of this process is the recruitment of osteogenic cells from vascular connective tissue around the implant where these cells migrate toward the surface topography using fibrin scaffold as migratory pathway [15], in agreement with previous studies that evaluated a clear correlation between surface roughness and human fibrin clot retention [12, 16, 17].

The micro-design obtained by laser-sintered solids resulted from the annealing and partial fusion of the roughly spherical particles of Ti-6Al-4V starting material at periphery of the powder bed where they cool more quickly than in the center [11]. In the DLMS micro-implants, the 3D environment of channels and pores of heterogeneous dimensions after acid etching using oxalic and maleic acids may be conductive to bone-to-implant contact. Additionally, several studies have been shown that acid treatment enhances early bone–implant integration to a level similar to that observed around the more complex surface topographies [18, 19]. In addition, the histologic ground sections depicted osteoblasts lining the newly formed bone on DLMS surface.

In addition, it could be hypothesized that bone formation within the cavities of the DLMS topography occurs when osteoblast precursors migrating into pores of the rough surface reach confluence earlier within the enclosed spaces, cease proliferation, and then differentiate [20], while growth factors may become concentrated within cavities, as demonstrated in the case of bone morphogenetic protein and hydroxyapatite [21, 22]. In a previous study [12], cells appeared to adhere mainly to the protruding, rounded features, and extended between them, creating a biological architecture superimposed on that of the DLMS surface, which could in theory facilitate macromolecule concentration at the implant surface, as proposed earlier. The differential cell adhesion could be related to higher surface tension in these regions than in the depressions, which could in turn influence protein adsorption and hence cell adherence [23].

On the other hand, SEM and EDX analysis showed a close relation between newly formed bone matrix and DLMS surface. The elemental analysis of the bone tissue revealed the presence of calcium and phosphorus suggesting mineralized bone tissue on titanium surface. This observation demonstrates that the DLMS surface could provide an optimal stratum to the bone tissue ingrowths. The SEM analysis agrees with the histological features where there is a new bone matrix over the implant surface. The proliferation and differentiation of bone cells has been reported to be enhanced by roughness of the implant surface topography [24, 25]. The healing is initiated immediately after implant insertion by initial blood clot formation in the peri-implant gaps and the development of a layer of fibrins [15, 16]. In addition, a series of coordinated events, including protein adsorption, proliferation, and deposition of bone tissue were probably affected by the different topography surfaces. The higher roughness of the DLMS surface could provide a better condition for coagulum stability, facilitating the bone healing on the implant surface.

Within the limits of these histological case series, it may be suggested that direct laser fabrication provides around 60% of bone-to-implant contact under unloaded conditions. However, further studies should be conducted to evaluate the long-term prognosis of these implants under occlusal loading.

References

1. Roach P, Eglin D, Rodhe K, Perry CC (2007) Modern biomaterials: a review—bulk properties and implications of surface modifications. J Mater Sci Mater Med 18:1263–1277
2. Shibli JA, Grassi S, Piattelli A et al. (2009) Histomorphometric evaluation of bioceramic molecular impregnated and dual acid-etched implant surfaces in human posterior maxilla. Clin Implant Dent Related Res. doi:10.1111/j.1708-8208.2009.00174.x
3. Grassi S, Piattelli A, de Figueiredo LC et al (2006) Histologic evaluation of early human bone response to different implant surfaces. J Periodontol 77:1736–1743
4. Shibli JA, Grassi S, de Figueiredo LC, Feres M, Marcantonio E Jr, Iezzi G, Piattelli A (2007) Influence of implant surface topography on early osseointegration: a histological study in human jaws. J Biomed Mater Res B Appl Biomater 80:377–385
5. Ivanoff CJ, Widmark G, Johansson C, Wennerberg A (2003) Histologic evaluation of bone response to oxidized and turned titanium micro-implants in human jawbone. Int J Oral Maxillofac Implants 18:341–348
6. Ivanoff CJ, Hallgren C, Widmark G, Sennerby L, Wennerberg A (2001) Histologic evaluation of the bone integration of TiO_2 blasted and turned titanium microimplants in human. Clin Oral Implants Res 12:128–134
7. Lopez-Heredia MA, Goyenvalle E, Aguado E et al (2008) Bone growth in rapid prototyped porous titanium implants. J Biomed Mater Res A 85:664–673
8. Mullen L, Stamp RC, Brooks WK, Jones E, Sutcliffe CJ (2009) Selective laser melting: a regular unit cell approach for the manufacture of porous, titanium, bone in-growth constructs, suitable for orthopedic applications. J Biomed Mater Res B Appl Biomater 89:325–334
9. Banhart J (2001) Manufacture, characterization and application of cellular metals and metal foams. Prog Mater Sci 46:559–632
10. Abe F, Osaka K, Shiomi M, Uematsu K, Matsumoto M (2001) The manufacturing of hard tools from metallic powders by selective laser melting. J Mater Process Technol 111:210–213
11. Traini T, Mangano C, Sammons RL, Mangano F, Macchi A, Piattelli A (2008) Direct laser metal sintering as a new approach to fabrication of an isoelastic functionally graded material for manufacture of porous titanium dental implants. Dent Mater 24:1525–1533
12. Mangano C, Raspanti M, Traini T, Piattelli A, Sammons R (2008) Stereo imaging and cytocompatibility of a model dental implant surface formed by direct laser fabrication. J Biomed Mater Res A. doi:10.1002/jbm.a.32033
13. Santos EC, Shiomi M, Osaka K, Laoui T (2006) Rapid manufacturing of metal components by laser forming. Int J Mach Tools Manuf 46:1459–1468
14. Piattelli A, Scarano A, Quaranta M (1997) High-precision, cost-effective system for producing thin sections of oral tissues containing dental implants. Biomaterials 18:577–579
15. Davies JE (1998) Mechanisms of endosseous integration. Int J Prosthodont 11:391–401
16. Di Iorio D, Traini T, Degidi M, Caputi S, Neugebauer J, Piattelli A (2005) Quantitative evaluation of the fibrin clot extension on different implant surfaces: an in vitro study. J Biomed Mater Res B Appl Biomater 74:636–642
17. Park JY, Gemmell CH, Davies JE (2001) Platelet interactions with titanium: modulation of platelet activity by surface topography. Biomaterials 22:2671–82
18. Klokkevold PR, Johnson P, Dadgostari S, Caputo A, Davies JE, Nishimura RD (2001) Early endosseous integration enhance by dual acid etching of titanium: a torque removal study in the rabbit. Clin Oral Implant Res 12:350–357
19. Buser D, Nydegg T, Oxland T et al (1999) Interface shear strength of titanium implants with a sandblasted and acid etched surface: a biomechanical study in the maxilla of miniature pigs. J Biomed Mater Res 45:75–83
20. Stein GS, Lian JB, Owen TA (1990) Relationship of cell-growth to the regulation of tissue-specific gene-expression during osteoblast differentiation. FASEB J 4:3111–3123
21. Ripamonti U (2004) Soluble, insoluble and geometric signals sculpt the architecture of mineralized tissues. J Cell Mol Med 8:169–180
22. Ripamonti U (1996) Osteoinduction in porous hydroxyapatite implanted in heterotopic sites of different animal models. Biomaterials 17:31–35
23. Faghihi S, Bateni MR, Azari F, Szpunar JA, Vali H, Tabrizian M (2005) The role of crystallographic texture of Ti-6Al-4V alloy on cell attachment and proliferation. Icotom 14: Textures Mater (Parts 1 and 2); 705–710
24. Martin JY, Schwartz Z, Hummert TW, Schraub DM, Simpson J, Cochran DL (1995) Effect of titanium surface roughness on proliferation, differentiation and protein synthesis of human osteoblast-like cells. J Biomed Mater Res 29:389–401
25. Schwartz Z, Lohmann CH, Oefinger J, Bonewald LF, Dean DD, Boyan BD (1999) Implant surface characteristics modulate differentiation behavior of cells in the osteoblastic lineage. Adv Dent Res 13:38–48